RSC Advances

ROYAL SOCIETY OF CHEMISTRY

www.rsc.org/advances

Enhanced Shape Memory Performance of Polyurethanes via the Incorporation of Organic or Inorganic Networks

Chien-Hsin Wu[1], Shi-Min Shau[2], Shin-Chih Liu[2], Shenghong A. Dai[2], Su-Chen Chen[3], Rong-Ho Lee[2]*, Chi-Fa Hsieh[4], and Ru-Jong Jeng[1]*

[1] Institute of Polymer Science and Engineering, National Taiwan University, Taipei 106, Taiwan

[2] Department of Chemical Engineering, National Chung Hsing University, Taichung 402, Taiwan

[3] Department of Energy and Materials Technology, Hsiuping University of Science and Technology, Taichung 412, Taiwan

[4] Chung-Shan Institute of Technology, Lungtan, Taoyuan 325, Taiwan

*Corresponding authors. RHL, Tel.: +886-4-2285-4308; Fax: +886-4-2285-4734 ; RJJ, Tel.: +886-2-3366-5884; Fax: +886-2-3366-5237

E-mail: rhl@dragon.nchu.edu.tw (RHL) ; rujong@ntu.edu.tw (RJJ)

ABSTRACT

A diol compound with reactive azetidine-2,4-dione group was prepared and introduced as side chain moieties of poly(ε-caprolactone) (PCL) based polyurethane (PU). The PUs with reactive pendants were crosslinked by 1,6-diaminohexane, or modified by an alkoxysilane (3-aminopropyltriethoxysilane, APTS) followed by a sol-gel reaction to bring about crosslinked PUs for shape memory applications. Thermal and mechanical properties of the crosslinked PUs are strongly dependent on the chemical structure of the interchain-linker between the polymer chains. Higher tensile strengths would be achieved for the PU samples crosslinked with alkoxysilanes in comparison with the ones crosslinked with an aliphatic diamine, while higher values of elongation at break were observed for the latter. As compared to the PCL based linear and side-chain PUs, much better shape memory performance was observed as the PU sample was crosslinked with the aliphatic diamine, or by the sol-gel reaction of alkoxysilanes, particularly the latter. Higher shape retention (91%) and recovery (99%) ratios were observed for the CPU samples with inorganic networks. By introducing the chemically crosslinked structures, the deformed PU samples completely recovered their original shape in less than 10 second without any deficiency during shape recovery measurements.

Keywords: azetidine-2,4-dione, organic/inorganic hybrid, shape memory polyurethane.

1. Introduction

Smart polymers, which can undergo large scale shape or property changes in response to external stimulus, such as stress, temperature, light or pH, have attracted great interest [1]. Among them, the thermo-responsive shape memory polyurethane (PU) is one of the most widely studied stimuli-responsive materials [2, 3]. PUs can be easily deformed into a temporary shape when heated, and fixed at the temporary shape after fast cooling down, and then regain their original shape upon heating again. Linear PUs (LPUs) with noteworthy phase separation of the soft- and hard-segment domains might exhibit certain shape memory effects [2]. Hard segment based domains play an important role in the recovery of the polymer shape above the melting point (T_m) of soft segment domains, while the soft segment domains based amorphous phase absorb the external stress and keep the polymer resilience at low temperatures. Four approaches have been set forth to overcome poor recovery ratio and mechanical properties of PUs by developing either chemical or physical modifications: (1) adjusting the hard-to-soft segment ratio [4-7], (2) enhancing the strength and number of ionic forces or hydrogen bonding [8, 9], (3) incorporating crosslinking networks [10, 11], and (4) blending with inorganic materials or creating organic/inorganic hybrids [12,13]. These shape memory polymers with biocompatibility and biodegradability have been found to possess high potential for biomedical applications, such as endovascular stroke treatment, cardiac valve repair, tissue engineering, drug delivery system, sensors and actuators, and pneumatic artificial rubber muscle [14-18]. Because of the ability of SMPs to perform complex movements on demand, many researchers are also pursuing high-tech applications including aerospace, active disassembly, adhesive systems, and energy storage, and so on [19-22].

In order to enhance the shape memory performance, the PUs with different kinds of organic segments or inorganic units based crosslinking networks have been developed (Fig. 1) [23-33]. Chun et al reported a new crosslinking approach in which the shape memory PU chains were crosslinked laterally by a flexible poly(ethylene glycol) (PEG) spacer between the polymer chains (Fig. 1(a)) [23,

24]. Each polymer chain was laterally connected by a spacer, and became stronger when stretched. The shape fixity and shape recovery of more than 80-90% were obtained for these PEG crosslinked PUs [23,24]. The PUs laterally crosslinked with hard segment methylene diphenyl diisocyanate (MDI) was reported by Chung et al. (Fig. 1(b)) [25]. High shape recovery and low shape retention were observed for these PUs. In addition, Hu et al. reported that suitable multifunctional monomers were introduced during the PU prepolymerization stage to provide three-dimensional networks of PUs (Fig. 1(c)) [26]. With an increase in the chemical crosslinking density, these crosslinked PUs (CPUs) with high storage modulus in rubbery state would provide enough force to recover to their original shape when they are heated to the temperatures above T_m of soft segment domains [26]. In addition to the organic crosslinker, the shape memory performance of the CPU with inorganic network was also investigated [27-33]. Cho et al. reported that a shape memory PU was mixed with tetraethoxysilane (TEOS), and a sol-gel reaction was followed to form a PU-silica composite (Fig. 1(d)) [27]. The shape fixity and shape recovery of more than 80% were obtained for these PU-silica nanocomposites. Moreover, 3-aminopropyltriethoxysilane (APTS) was attached to PU as side group through an allophanate bonding site (Fig. 1(e)) [28]. The PUs were crosslinked by the sol-gel reaction between the triethoxysilyl groups via acidic hydrolysis. Due to a limited triethoxylsilane content, the sol-gel reactions did not provide extensive inorganic networks. As a result, low tensile strength and high elongation at break were observed for the PUs with polysiloxane linkages. In addition, the APTS acting as chain extender and crosslinker was reacted with a PU prepolymer end-capped with epoxide functional groups (Fig. 1(f)) [29]. Subsequently, shape memory PU–silica nanohybrids were prepared by sol–gel reactions between the surface silanol groups of fumed silica and hydrolyzed alkoxysilanes of the PU. As a result, significantly enhanced reinforcing effects (modulus and strength) were obtained as compared with the PUs crosslinked by sol-gel reactions without the addition of fumed silica particles. High shape retention and recovery ratios were observed for the PU laterally crosslinked with fumed silica particles through sol-gel reactions [29]. Bae et al. introduced silica nanoparticles (1–5 wt%) into an amorphous PU, which allowed one to control the glass transition temperature (T_g) (Fig. 1(g)) [30]. To

further improve the compatibility and reduce the size of micro-domains, the PU was end-capped with APTS, and a sol–gel reaction with silica particles was followed. The silica particles acting as the multifunctional crosslinkers as well as reinforcing fillers would significantly enhance the tensile strength and shape memory properties. Apart from that, the PCL functionalized inorganic units, such as SiO_2 microspheres and polyhedral oligomeric silsesquioxane (POSS), were crosslinked with the diisocyanate derivative, and the resultant CPU/inorganic nanohybrids were used for shape memory applications (Fig. 1(h)). Excellent mechanical strength and good shape memory properties were observed due to the introduction of the SiO_2 microspheres and POSS units [31-33].

Accordingly, the incorporation of crosslinking network could enhance the shape memory performance of PUs. In this study, we synthesized a di-para-phenyl isocyanate (MDI) based building block, 4-isocyanate-4′-(3,3-dimethyl-2,4-dioxo-azetidine)diphenyl methane (IDD) with dual functionalities according to the literature [34-37]. By adopting a reactive diol derived from the building block IDD as starting material, a facile synthesis of reactive side-chain PU (SPU) consisting of MDI hard segment, soft segment of PCL, and pendant reactive azetidine-2,4-dione group was achieved. The azetidine-2,4-dione functional group exhibits selective reactivity only toward aliphatic primary amines. Because of this, the PU with pendent azetidine-2,4-dione groups could be crosslinked by an aliphatic diamine (1,6-diaminohexane), or modified by APTS followed by the sol-gel reaction to bring about a PU-silica hybrid for shape memory applications. The crosslinking density of CPUs could be controlled by the addition of crosslinker content (i.e. aliphatic diamine or APTS). The effects of hard segment content, and organic and inorganic crosslinkers on the mechanical and shape memory properties were investigated. The PUs laterally crosslinked by a short segment (1,6-diaminohexane) would exhibit better flexibility in terms of facile property-tuning as compared to those of the PUs crosslinked by a multifunctional monomer, flexible long segment (PEG), and hard segment MDI [23-26]. Moreover, the approach of PU-silica hybrids prepared by direct sol-gel reaction of the APTS attached PUs is quite different from that of the hybrids prepared by the sol-gel reaction of alkoxysilane with fumed silica particles [29-33]. These PUs laterally crosslinked with hydrogen bond-rich

malonamide moieties containing short organic or hard inorganic interchain linkers would certainly exhibit better morphology, mechanical properties, and shape memory properties as compared to those of the crosslinked PUs reported in literature.

2. Experimental

2.1. Materials

Methylene di-p-phenyl diisocyanate (MDI), isobutyryl chloride, diethylene glycol (DEG), diethanolamine (DEA), 1,6-diaminohexane, catalyst dibutyltin dilaurate (T-12) and 3-aminopropyl triethoxysilane (APTS) were all reagent grade from Aldrich and used as received. Triethylamine (TEA) and 1, 2-ethylenediamine (EDA) were purchased from TEDIA. Acetic acid (AcOH) 95% in water was obtained from Scharlau. Xylene, tetrahydrofuran (THF), dimethylformamide (DMF), acetone, and cyclohexane were distilled under reduced pressure over CaH_2 and stored over 4 Å molecular sieves. Polycaprolactone diol (PCL 2303, Mn = 3000), which is a caprolactone based difunctional polyester polyol, purchased from Perstorp Specialty Chemicals Company, was dried and degassed at 80 ^{o}C, 1–2 mm Hg for 4 h before use. IDD-diol, LPU, SPU, and CPUs were synthesized as shown in Schemes 1-3. Formulations of the LPUs, SPUs, and CPUs are summarized in Table 1.

2.2. Synthesis of IDD-diol

In Scheme 1, the building block, 4-isocyanate-4′-(3,3-dimethyl-2,4-dioxo-azetidine)diphenyl methane (IDD) was synthesized according to procedures described in the literature [34]. Diethanolamine (3 g, 28.57 mmol) was added to a solution of IDD (11.4 g, 35.63 mmol) in dry THF (25 mL). The solution was stirred at 0 ^{o}C under a nitrogen atmosphere for 5 h. The resulting solution was concentrated to paste, collected and crystallized from cyclohexane. The white powder of IDD-diol was obtained with a yield of 85%. FTIR (KBr, cm^{-1}): 3305 (-OH), 1855(C=O), 1740 (C=O), 1638 cm^{-1} ((NH)C=O(N)); ^{1}H NMR (δ/ppm, DMSO-d_6): 1.39 (s, 6H, –CH_3), 3.33 (t, 4H, –CH_2–), 3.56 (t, 4H, –CH_2–), 3.86 (s, 2H, Ar–CH_2–Ar), 5.07 (s, 2H, –OH), 7.02–7.12 (d, 2H, Ar–H), 7.13–7.40 (d, 4H, Ar–

H), 7.41–7.72 (m, 2H, Ar–H), 8.61 (s, H, Ar–NH–C=O); Anal. calcd for $C_{23}H_{27}N_3O_5$: C, 64.79; H, 6.34; N, 9.86; Found: C, 64.83; H, 6.40; N, 9.88; MS: m/z (FAB) 426 [M^+].

2.3. Preparation of LPUs, SPUs, and CPUs

In Scheme 2, different compositions of PUs were synthesized via a two-step condensation reaction. The reaction was carried out by adding MDI to a solution of PCL in dry DMF. The reaction solution was heated at 60 ^oC for 0.5 h to obtain isocyanate terminated prepolymer. Subsequently, the chain extender DEG or IDD-diol was added dropwise into the stirring reaction at 80 ^oC for 3 h to obtain LPUs or reactive type SPUs (designated as LPU-xx and SPU-xx, respectively, where xx is the hard segment content, wt%), respectively The as-polymerized solution (10 wt%) was poured into Teflon circular disks at room temperature for 24 h and then heated to 60−70 ^oC for an additional 48 h under vacuum. Thick film was obtained on the order of 5 mm thick. The formulations of the LPUs and SPUs with different content of hard segments are summarized in Table 1. The weight-average molecular weights (Mw) of LPUs and SPUs were ranged from 4.73 × 10^4 to 14.4 × 10^4 (g/mol) with polydispersities between 2.2 and 4.4 (Table 1).

The prepared SPUs mentioned above were directly crosslinked via the addition of 1,6-diaminohexane (Scheme 3). Crosslinking networks were formed through the ring-opening reaction of azetidine-2,4-diones toward the primary amine (designated CPU-Axx, where xx is the diamine content, mol.% (to the content of ADD-diol). As shown in Scheme 3, the azetidine-2,4-dione containing SPUs were also further modified with 20, 40 and 60 mol.% (to the content of IDD-diol) of APTS, respectively. The APTS grafted SPUs were then treated with water/acetic acid at the ratio of H_2O: HOAc: APTS = 0.0014: 0.007: 1 (molar ratio), undergoing the sol-gel reaction. The solution was stirred at room temperature for 1 h and poured into Teflon disks at room temperature for 24 h, and then heated to 60−70 ^oC for an additional 48 h under vacuum (designated CPU-Sxx, where xx is the APTS content, mol.% (to the content of ADD-diol). The formulations of the CPUs with different content of crosslinking agents are summarized in Table 1.

2.4. Methods

^{1}H NMR spectra were taken on a Varian Gemini-200 FT-NMR spectrometer with chloroform-d and dimethyl sulfoxide-d_6. Elemental analysis was performed on a Heraeus CHN-OS Rapid Analyzer. Infrared spectra were recorded to identify the chemical structure of PUs using a Jasco 4100 FT-IR Spectrophotometer. Infrared spectra were measured with a Jasco ATR Pro 450-S accessory. Gel permeation chromatography (GPC) was performed using a Waters chromatography system, two Waters Styragel linear columns, and polystyrene as the standard. THF was used as the eluent at a flow rate of 0.84 mL/min at 40 ^{o}C. Glass transition temperatures (T_g), recrystallization temperature (T_c), and melting temperature (T_m) were measured under a N_2 atmosphere using a differential scanning calorimeter (TA Instruments, DSC-2010) operated at a heating rate of 10 °C min^{-1}. The transition temperatures were obtained from the second heating scan. Thermogravimetric analysis (TGA) was performed under a N_2 atmosphere using a Thermo Electro Co. Thermo Cahn thermogravimetric analyzer operated at a heating rate of 10 °C min^{-1}. Dynamic mechanical analysis (DMA) was performed using a PerkinElmer SII Diamond DMA instrument. The width and length of the strip PU specimens for mechanical tests were about 5 and 20 mm, respectively. The values of storage moduli (E'), loss moduli (E'') and tan δ were determined for PU samples (thickness, ~40 μm) that had been subjected to the temperature scan mode at a programmed heating rate of 2 °C/min under a N_2 atmosphere from −100 to 150 °C at a frequency of 1 Hz and an amplitude of 15 μm. Tensile strength measurements were carried out using a Gotech testing machine (AI-3000, Gotech Detection Device Co., Ltd., Taiwan) with a cross-head speed of 100 mm/min. Dumbbell-shape tensile specimens were made according to ASTM D638 specification [28, 38]. The tensile tester equipped with a temperature controlled chamber (GT-7001-HL) was also utilized to study the shape memory effect of the PUs. Shape memory behavior was examined by cyclic thermomechanical tensile tests. The heating and cooling rate were controlled at 2 ^{o}C/min. The specimen was loaded to the strain (ε_m: 100%) at a constant crosshead speed of 10 mm/min at deformation temperature (T_{def}, 70 ^{o}C), that is 30 ^{o}C exceeding the melting temperature (T_m) of soft segment based domains (Process 1). Subsequently, it

was cooled to the fixing temperature (T_{fix}, 10 ^{o}C) under the same strain (Process 2) [26, 30, 39, 40]. After 10 min, the load on the specimen was taken off (holding for 5 min), the fixed strain (ε_u) was recorded (Process 3), then the specimen was heated from 10 ^{o}C to 70 ^{o}C, and the residual strain (ε_p) was recorded (Process 4). The shape fixity and shape recovery could be calculated based on the following equations:

Shape retention ratio (%) = ε_u / ε_m × 100.

Shape recovery ratio (%) = (ε_m – ε_p) /ε_m × 100.

3. Results and discussion

3.1. Synthesis and characterization of PUs

In this work, a reactive diol, IDD-diol was derived from IDD. As shown in Scheme 1, the azetidine-2,4-dione group of IDD-diol is highly reactive and readily undergoes ring-opening reaction with an aliphatic primary amine, forming a malonamide linkage [35]. Chemical structure of the resultant IDD-diol was fully confirmed by FTIR, ^{1}H NMR, elemental analysis, and Mass spectroscopy [42]. Moreover, chemical structures of LPUs, SPUs, and CPUs were characterized by FTIR Spectroscopy. FTIR spectra of LPU55, SPU55, CPU55-A10, and CPU55-S60 are shown in Fig 2. The absent of the absorption peak at 2260cm^{-1} confirms that the polymerization was completed for LPUs and SPUs. The characteristic absorption peaks of carbonyl groups corresponding to the ester and urethane groups were respectively observed at 1730 and 1705 cm^{-1} for LPU55. Typically, the hydrogen-bonded carbonyl group attributed to the urethane groups showed up at a lower absorption wavenumber (1705 cm^{-1}). Moreover, the crosslinkable SPUs were obtained by the incorporation of azetidine-2,4-dione containing IDD-diol as the crosslinkable group. For SPU55, the characteristic absorption peaks of azetidine-2,4-diones were observed at 1743 and 1855 cm^{-1}. The intensities of the absorption peaks were decreased significantly after 20% molar ratio of di-amine was reacted with the azetidine-2,4-dione groups (CPU55-A10). In addition, the absorption peak of malonamide was appeared at 1650 cm^{-1}. This indicates that the facile ring-opening reactions of the azetidine-2,4-dione groups with the aliphatic primary amines occurred and the malonamide linkages were formed. On the

other hand, the absorption peak of azetidine-2,4-diones was completely disappeared by incorporating of APTS for CPU55-S60. Before the sol-gel reaction, the absorption band of the silanol stretching was observed at 955 cm^{-1} for CPU55-S60. The intensity of this absorption band was decreased after sol-gel reaction. Moreover, the absorption peak at 1100 cm^{-1} became broader. This suggests the formation of Si–O–Si bonds [29, 30].

3.2. Thermal properties

Thermal stabilities of the PU samples were studied by using TGA. Degradation temperatures (T_ds) of the PUs are summarized in Table 2. Thermal stabilities of the SPUs (SPU45, SPU50, and SPU55) were lower than those of the LPUs (LPU45, LPU50, and PU55). This is due to the presence of the azetidine-2,4-diones in SPUs [43]. The weight loss at 200-280 ^oC was caused by the degradation of azetidine-2,4-diones for SPUs. In addition, the thermal stabilities of the crosslinked SPUs were slightly higher than those of the pristine SPU samples due to the formation of crosslinking networks [44]. On the other hand, thermal transitions of LPUs, SPUs, and CPUs were also determined by DSC. The DSC curves from the second heating runs are shown in Fig. 3. The T_gs, recrystallization temperatures of soft segment based domains (T_{cS}), recrystallization degree of soft segment based domains (X_{cS}), melting temperature of soft segment based domains (T_{mS}), crystallization degree of soft segment based domains (X_{mS}), and melting temperature of hard segment based domains (T_{mH}) for PUs are summarized in Table 2. For LPUs comprising 45−55% PCL segment, the T_gs were observed at about -48 ^oC, which were slightly higher than that of the pristine PCL (T_g ~ -62 ^oC) [45]. The T_gs of LPUs slightly increased with increasing hard segment content. In the second heating scan, a weak recrystallization peak was appeared at about −1.1 ^oC for LPUs, which is attributed to the crystallization of the soft segment based domains. As a result, the LPUs exhibited T_{mS} at about 37−44 ^oC, which was slightly lower than that of pristine PCL (ca. 47 ^oC) [45]. This is due to the decreased crystallinity of PCL segment and the inhibited crystal formation with the presence of hard segment. With increasing hard segment content, the T_{mS} peak became indistinct, and the T_{mH}

transition started to appear in Fig. 3(a). LPU50 and LPU55 with high hard segment contents exhibited clear T_{mH} peaks at about 145−150 ^{o}C (inset in Fig. 3 (a)) [46]. Based on the above, the phase separation of the LPUs is caused by the presence of incompatibility between the soft segment and hard segment based crystallites. Nevertheless, the crystallization degree of the hard segments is low for the LPU samples.

In addition, the T_gs of SPUs were observed at about -44 ^{o}C. The T_gs were enhanced by the incorporation of azetidine-2, 4-dione-containing chain extenders. The recrystallization and melting transition peaks of the soft segment based domains were observed at about 10 and 40 ^{o}C for SPUs, respectively. The T_{cS}, $X_{cS,}$ T_{mS}, and $X_{mS,}$ of the SPU samples were much higher than those of LPUs with the same hard segment content. However, no melting transition (T_{mH}) of hard segments based crystallites was observed for SPUs. This implies that the formation of hard segments based crystallites would be restricted by the presence of IDD-diol chain extenders. The crystallization behaviors of soft- and hard-segment based domains would interfere with each other due to the fact that the polymer chains were interpenetrating between different segment domains. The introduction of bulky pendants (IDD-diol chain extenders) inhibited the crystal formation in the hard segment based domains. Less crystallinity in hard segment domains is favorable for the recrystallization in the domains of PCL soft segments. This is because more flexibility is available for the soft segments to crystallize as the crystallinity of hard segments decreases. Apart from that, similar thermal behaviors were observed for CPUs by using 1,6-diaminohexane as the crosslinking agent in comparison with those of SPUs (Fig. 3(b)). However, the influence of the crosslinking structure on the thermal behaviors of PUs was more significantly for CPUs with APTS as the crosslinking agent. The X_{cS} and X_{mS} of the CPU samples crosslinked with the sol-gel reaction of alkoxysilanes were much lower than those of the SPUs, implying that the incorporation of the Si-O-Si segment based crosslinking units suppressed the recrystallization of the PCL based soft segments. This is confirmed by Paderni et al. that the crystallinity in the sol–gel crosslinked alkoxysilane-terminated PCL are mainly dependent on the length of PCL segment and the crosslinking density [39].

3.3. X-ray Diffraction (XRD)

As shown in Fig. 4, the morphologies of the LPU, SPU, and CPUs samples were characterized by using XRD patterns. A broad amorphous band ranged from 15 to 30^{o} was observed for the LPU45, LPU50, and LPU55, which is attributed to the low crystallinity of LPUs. In contrast, two sharp peaks were observed at 21.2^{o} and 23.6^{o} for the SPU45, SPU50, and SPU55. Two sharp diffraction peaks are attributed to the (110) and (200) diffractions of the soft segment based orthorhombic crystals and the hard segment based crystals [47]. As compared to LPUs, the presence of azetidine-2,4-dione based pendants is favorable for the recrystallization in PCL soft segment based domains. As a result, high crystallinity was observed for the SPU samples. In addition, the crystallinities of the soft- and hard-segment based domains were not decreased for the PUs laterally crosslinked with a flexible spacer, 1,6-diaminohexane. Two sharp diffraction peaks were also observed at 21.2^{o} and 23.6^{o} for CPU50-A05 and CPU50-A10. However, the crystallinities of the soft- and hard-segment based domains were reduced for the PUs laterally crosslinked with alkoxysilanes. As compared to SPUs, the intensities of the diffraction peaks were decreased for CPU55-S20, CPU55-S40, and CPU55-S60. The incorporation of inorganic crosslinks suppressed the recrystallization of PCL soft segment based domains. Therefore, lower crystallinity was observed for the alkoxysilane-crosslinked CPUs.

3.4. Mechanical properties

Stress-strain curves of various PUs with the same hard segment content (55%) are shown in Fig. 5. Five runs of tensile test were performed for each PU sample. The statistic values of tensile strength (σ_b), elongation at break (ε_b), elastic modulus (E_e), and secant modulus (E_s) for LPUs, SPUs, and CPUs are summarized in Table 3. In Fig. 5(a), the tensile strength, and elastic and secant moduli were increased with increasing hard segment content, which is ascribed to the accumulated interactions of a great many hydrogen bonding sites in hard segment based domains. The elongation at break, however, showed the opposite tendency as the hard segment content of LPUs increased. With a highest hard segment content, LPU55 exhibited excellent elastic-plastic behavior pertaining to the tensile strength (107.0 MPa) and elongation (423%) at break. For SPUs, the tensile strength,

elongation at break, and elastic and secant moduli were poorer than those for LPUs (Fig. 5(a)). The incorporation of reactive pendants resulted in the decrease of the mechanical properties for SPUs. Moreover, the tensile strength increased with increasing hard segment content, while the elongation at break showed the opposite trend.

In addition, mechanical properties were also affected by the crosslinking density of CPUs. Tensile strengths, and elastic and secant moduli of the CPUs were enhanced with increasing crosslinking density, while the elongation at break showed otherwise (Fig. S2, Supporting Information). In Fig. 5(b), much higher tensile strengths were observed for the SPU55 samples crosslinked with alkoxysilanes (CPU55-S20, CPU55-S40, and CPU55-S60) in comparison with the ones crosslinked with 1,6-diaminohexane (CPU55-A05 and CPU55-A10). The incorporation of inorganic crosslinkers between the backbones of PUs resulted in the high tensile strengths and low elongation at break for CPU55-S20, CPU55-S40, and CPU55-S60. The presence of an excess of silicon oxide networks hinders the deformation of soft-segments in PUs and thus leads to lower elongation at break [27]. In contrast, higher values of elongation at break were observed for the SPU55 samples crosslinked with 1,6-diaminohexane in comparison with the ones crosslinked with alkoxysilanes. The presence of flexible alkyl chain in 1,6-diaminohexane as interlink-segments showed high extension behavior for the crosslinked SPU samples.

It is important to note that higher tensile strengths, and larger elastic and secant moduli were observed for CPU55-S40 and CPU55-S60 as compared to that for LPU55 as the PU samples with 55% hard segment were stretched to 100% elongation (Table 3). The synergistic effect of physical crosslinking of hard segments and chemical crosslinking of inorganic interlink-segments resulted in higher elastic and tensile strengths of CPU55-S40 and CPU55-S60. The tensile strengths of these CPUs laterally crosslinked with alkoxysilanes are comparable to those of the CPU samples with the addition of fumed silica particles [29, 30]. Apart from that, higher tensile strengths were observed for the CPUs (CPU55-A05 and CPU55-A10) using a short flexible spacer (1,6-diaminohexane) as

crosslinker as compared to those for the CPUs crosslinked with a poly(ethylene glycol) spacer, while the latter shows larger elongations at break than the former ones [23, 24]. Based on the above, the tensile properties are affected by the hard segment content and the degree of crosslinking.

3.5. Dynamic mechanical properties

Dynamic mechanical analysis and shape recovery tests revealed the relationship between shape memory behaviors and polymeric structures. Temperature dependence of the storage modulus (E′) and tan δ curves of PUs obtained from DMA are presented in Fig. 6. In Fig. 6(a), a decrease of E′ was observed at temperature ranged from -40 to 0 ^{o}C for LPU55, which is corresponding to the molecular motion above T_g. However, the formation of the crystallites in soft-segment domains led to an observation of a weak tanδ peak at about -20 ^{o}C for LPU55 (Fig. 6(b)). At temperatures higher than 20 ^{o}C, the E′ value was not decreased significantly with increasing temperature, which is attributed to the presence of the hard-segment crystal domains. The presence of the crystal domains resulted in high E′ values at temperatures above the T_m of the soft segment based domains. Similar dynamic mechanical properties were observed for LPU45 and LPU50. In addition, the temperature dependence of E′ curves were quite different for SPU55 and CPUs in comparison with that for LPU55 (Fig. 6(a)). At temperatures lower than 20 ^{o}C, the E′ values of SPU55 and CPUs were higher than that of LPU55. The recrystallization of soft segments and/or the crosslinking effect resulted in higher E′ values of SPU55 and CPUs. Moreover, the E′ value decreased significantly with increasing temperature corresponding to the melting of the soft-segment crystal domains. As a result, lower E′ values were observed for SPU55 and CPUs as the temperature reached 40 ^{o}C. Furthermore, the relaxation temperatures of the tanδ peaks were observed at temperatures higher than 40 ^{o}C for SPU55 and CPUs (Fig. 6(b)). The relaxation intensities of SPU55 and CPUs were much larger than that of LPU55. In addition, the intensities of tanδ peaks for CPUs were lower than that for SPU55. The molecular motion was suppressed after the PU samples crosslinked with 1,6-diaminohexane or alkoxysilanes.

The statistic values of moduli in the glassy region (E'_g) and rubbery region (E'_r), and the maximal tanδ ($tan_{max}\delta$) for PUs are summarized in Table 3. Five runs of dynamic mechanical analysis were performed for each PU sample. Shape memory behavior is strongly dependent on the dynamic mechanical properties. High E'_g values accounts for the temporary shape fixed at low temperatures, while reasonably low E'_r and high $tan_{max}\delta$ values lead to the faster shape recovery speed at high temperatures. For LPUs, an increase of hard segment content resulted in an increase of the moduli in glassy (E'_g) and rubbery (E'_r) state, while the tanδ values showed an opposite trend. Higher hard segment content would suppress the molecular motions during the glass transition of LPUs. In addition, the E'_g values of SPUs are much higher than those of LPUs. The incorporation of reactive pendants with high rigidity resulted in higher E'_g values of SPUs in glassy state. Better shape retention ratios were expected for SPUs in comparison with those of LPUs. However, the presence of reactive pendants would possibly reduce the packing density of polymer backbone. This led to larger $tan_{max}\delta$ and lower E'_r values of SPUs as compared to those of LPUs. The polymer with an optimized upper limit of E'_r value exhibits better shape memory effects for faster high temperature deformation and higher recovery speed in rubbery state [47-49]. As compared to SPUs, relatively high E'_g and E'_r values were obtained for CPUs, and proportionally enhanced with increasing crosslinking density. Inversely, the $tan_{max}\delta$ values of CPUs were lower than those of SPUs. In addition, the presence of network structures would enlarge the shape recovery force for CPUs [26]. Therefore, good shape memory properties would be obtained for CPUs with high E'_g values and large E'_g/E'_r ratios. Apart from that, the crosslinking effect on the mechanical properties of PUs was more significantly for the SPU samples crosslinked with alkoxysilanes as compared to the SPU samples crosslinked with 1,6-diaminohexane. The presence of the inorganic interlink-segments suppressed the molecular motions as the temperature was increased above the melting point of the soft-segment based crystals. Therefore, higher E'_r and lower $tan_{max}\delta$ values were observed for the SPU samples crosslinked with alkoxysilanes as compared to those for the SPU samples crosslinked with 1,6-diaminohexane.

3.6. Shape memory behavior

Shape memory behavior was examined by cyclic thermomechanical tensile tests. The samples were elongated to a strain of 100% at a stretching rate of 10 mm/min. The stress-strain curves of PUs are shown in Fig. 7. According to the cyclic thermomechanical tensile tests, the statistic values of shape retention and recovery for PUs are summarized in Table 4. Five runs of tensile test were performed for each PU sample. At elevated temperatures, the PU film usually softened and became a viscous liquid when the hard segment content of the PU sample was less than 40 wt%. The hard segments of PUs play an important role of providing sufficient physical interactions to sustain permanent shape. Moreover, the soft segments act as the switching components to fulfill external influence and memorize temporary shape after the deforming progress. For LPUs, just like the E'_g values, the shape retention was not changed significantly with increasing hard segment content. The shape retention is closely related to the storage modulus of PU in glassy state. The small variations of the E'_g values did not result in much difference in shape retention properties for LPUs. On the other hand, the shape recovery was slightly enhanced with increasing hard segment content corresponding to the increase of the E'_r values. Higher storage modulus in rubbery state provides the larger shape recovery force [26]. However, the shape recovery and retention were decreased after the second and third stretching scans as compared with the first ones. The stress-strain curves showed that the stress values were depressed after the second and third stretching scans, indicating that certain inner structure was remarkably destroyed or the entanglement of polymer chains was unwound during the stretching processes [32, 49]. In addition, the shape memory behaviors of the SPUs (SPU45, SPU50, and SPU55) were improved by the incorporation of the reactive pendants. Moreover, the SPU50 and SPU55 with higher hard segment contents showed better shape memory performance than did SPU45. The decrease of the shape recovery and retention of SPUs after the second and third stretching scans was suppressed when compared with those of LPUs. This implies that the inner structure of the polymer was only slightly destroyed after the stretching scans. With an increase in the hard segment content, the SPU can endure a higher level of stress above the T_ms on account of the presence of more physical crosslinking points [26, 32]. Although the shape memory behavior of PCL based PUs was somewhat

improved by the incorporation of reactive pendants, more effort has to be made on enhancing the recovery stress and E'_r value in rubbery state.

For the 1,6-diaminohexane crosslinked CPUs (CPU45-A05, CPU45-A10, CPU50-A05, CPU50-A10, CPU55-A05, and CPU55-A10), the shape recovery ratios were significantly improved with increasing content of interchain crosslinker, especially for the CPU samples with lower hard segment contents. However, the shape retention ratios did not vary significantly with different contents of interchain crosslinkers. This is possibly because the shape recovery and retention are opposite properties, shape retention is sacrificed as shape recovery increases [25]. Apart from that, the decreases of stress values after the second and third stretching scans became less significant for the CPU samples with increasing contents of hard-segment and interchain crosslinker. Moreover, the shape memory stress-strain curves show that the stress values remained virtually unchanged after the second and third stretching scans for CPU55-A10, indicating that the inner structure was intact during the stretching processes. It is important to note that the shape recovery and retention of the CPU samples (CPU50-A05, CPU50-A10, CPU55-A05, and CPU55-A10) using a short flexible spacer (1,6-diaminohexane) as crosslinker are better than those of the CPUs crosslinked with poly(ethylene glycol) spacer or MDI based short hard segment [23-25]. This is due to the presence of hydrogen bond-rich three dimensional networks. Furthermore, excellent shape memory performance was observed for the alkoxysilane crosslinked CPU samples (CPU55-S20, CPU55-S40, and CPU55-S60). Excellent shape retention and recovery were observed for these CPU samples. The shape recovery of Si-O-Si crosslinked hybrid CPU55-S60 was increased to over 99%. Higher E'_g values of CPUs resulted in the better shape retention than those of LPUs and SPUs. In addition, higher rubbery state moduli, E'_rs led to larger recovery stresses of alkoxysilane crosslinked PUs in comparison with the PU samples crosslinked with flexible aliphatic diamines. By incorporating the crosslinked structure based on hard inorganic Si–O–Si networks, higher storage moduli promoted the shape recovery properties. This indicates that the inorganic crosslinker plays an important role for the enhancement of shape

memory performance. However, some of the shape retention ratios did not vary significantly with increasing content of inorganic crosslinkers, which is attributed to the fact that these CPU samples exhibited similar E'_g values at temperatures below T_ms (Fig 6(a)). In addition to the above mentioned, the shape memory properties of PU-silica hybrids prepared by direct sol-gel reaction of the APTS attached PUs (CPU55-S20, CPU55-S40, and CPU55-S60) are comparable to those of the hybrids prepared by the sol-gel reaction of alkoxysilane with fumed silica particles, which is presumably due to the presence of hydrogen bond-rich malonamide moieties in the interchain linkages [29, 30].

The shape memory test was employed to evaluate the shape fixity and shape recovery performances (Supporting Information). As shown in Fig. 8, the shape recovery progressing from the temporary shape to the original shape at T_{def} was recorded by a digital camera [23, 40]. The shape recovery time of the deformed PU samples are shown in Fig. 9. At the beginning, all samples showed excellent shape fixity with the preservation of circle frames, indicating that the motions of the polymer chains in amorphous networks were frozen at T_{fix}. As the time went along, rapid shape recovery was observed for the CPU samples. These samples could regain their original shapes with the degree of almost 100% at T_{def}. In contrast, the deformed LPU and SPU samples were unable to fully recover even after a long period of time, especially for the SPU samples. The unreinforced fixing phase present in LPUs and SPUs would typically result in a long recovery time. On the other hand, the CPU samples could effortlessly achieve complete recovery without any deficiency and their shape-recovery rates were found to increase with increasing crosslinker content. Better shape memory polymers by employing organic or inorganic interlink-segments have been achieved.

4. Conclusion

In this study, PUs with reactive pendants were laterally crosslinked by a flexible spacer, 1,6-diaminohexane, or modified by alkoxysilanes followed by a sol-gel reaction to bring about PU-silica hybrids for shape memory applications. After crosslinking reactions, abundant hydrogen bond-rich three dimensional networks were present throughout CPUs. Consequently, excellent shape memory

performance was observed for the CPU samples. Better shape memory performance was observed for the PU sample crosslinked by the sol-gel reaction of alkoxysilanes as compared to the sample crosslinked with1,6-diaminohexane. The shape memory test indicates that the CPU samples could effortlessly achieve complete recovery without any deficiency and their shape-recovery rates were found to increase with increasing crosslinker content. Because of the presence of hydrogen bond-rich three dimensional networks, the shape recovery and retention of the CPU samples using 1,6-diaminohexane as crosslinker are better than those of the CPUs crosslinked with flexible long chain or short rigid linkage. In addition, the shape memory properties of PU-silica hybrids prepared by direct sol-gel reaction of the APTS attached PUs are comparable to those of the hybrids prepared by the sol-gel reaction of alkoxysilane with fumed silica particles.

Acknowledgments

We thank Chung-Shan Institute of Technology and Ministry of Science and Technology of Taiwan for financial support.

References:

1. J. Hu, Y. Zhu, H. Huang and J. Lu, *Prog. in Polym. Sci.*, 2012, **37**, 1720.
2. B. K. Kim, S. Y. Lee and M. Xu, *Polymer*, 1996, **37**, 5781.
3. Y. Shirai and S. Hayashi, *Mitsubishi Tech. Bull*., 1988, **184**, 1.
4. P. Ping, W. Wang, X. Chen and X. Jing, *Biomacromolecules*, 2005, **6**, 587.
5. M. Momtaz, M. R. Nouri and M. Barikani, *J. Mater. Sci.*, 2014, **49**, 7575.
6. M. Bothe, F. Emmerling and T. Pretsch, *Macromol. Chem. Phys.* 2013, **214**, 2683.
7. S. Weng, Z. Xia, J. Chen and L. Gong, *J. Appl. Polym. Sci.*, 2013, **127**, 748.
8. B. C. Chun, T. K. Cho and Y. C. Chung, *Eur. Polym. J.*, 2006, **42**, 3367.
9. S. Chen, J. Hu, C. W. Yuen and L. Chan, *Polymer*, 2009, **50**, 4424.
10. K. Hearon, K. Gall, T. Ware, D. J. Maitland, J. P. Bearinger and T. S. Wilson, *J. Appl. Polym. Sci.*, 2011, **121**, 144.
11. C. P. Buckley, C. Prisacariu and A. Caraculacu, *Polymer*, 2007, **48**, 1388.

12. M. Huang, X. Dong, Y. Gao, Q. Xing, W. Li and D. Wang, *Polymer*, 2014, **55**, 4289.
13. H. Meng and G. Li, *Polymer*, 2013, **54**, 2199.
14. W. S. IV, P. Singhal, T. S. Wilson and D. J. Maitland, *J. Mater. Chem.*, 2010, **20**, 3356.
15. A. M. Gumel and M. S. M. Annuar, *J. Appl. Polym. Sci.*, 2014, **131**, 41149.
16. H. Chen, Y. Li, Y. Liu, T. Gong, L. Wang and S. Zhou, *Polym. Chem.*, 2014, **5**, 5168.
17. G. Coativy, N. Gautier, B. Pontoire, A. Buleon, D. Lourdin and E. Leroy, *Carbohydrate Polymers*, 2015, **116**, 307.
18. K. Takashima, K. Sugitani, N. Morimoto, S. Sakaguchi, T. Noritsugu and T. Mukai, *Smart Mater. Struct.*, 2014, **23**, 125005.
19. Y. Liu, H. Du, L. Liu and J. Leng, *Smart Mater. Struct.*, 2014, **23**, 023001.
20. J. S. Kim, D. Y. Lee, J. S. Koh, G. P. Jung and K. J. Cho, *Smart Mater. Struct.*, 2014, **23**, 015011.
21. R. Wang and T. Xie, *Langmuir*, 2010, **26**, 2999.
22. M. Anthamatten, S. Roddecha and J. Li, *Macromolecules*, 2013, **46**, 4230.
23. B. Chun, T. Cho, M. Chong and Y. C. Chung, *J. Mater. Sci.*, 2007, **42**, 9045.
24. Y. C. Chung, T. K. Cho and B. C. Chun, *J. Appl. Polym. Sci.*, 2009, **112**, 2800.
25. Y. C. Chung, J. Choi, S. Shin and B. Chun, *Fibers Polym.*, 2012, **13**, 815.
26. J. Hu, Z. Yang, L. Yeung, F. Ji and Y. Liu, *Polym. Int.*, 2005, **54**, 854.
27. J. W. Cho and S. H. Lee, *Eur. Polym. J.*, 2004, **40**, 1343.
28. Y. C. Chung, N. Khiem, J. Choi and B. Chun, *J. Sol-Gel Sci. Technol.*, 2012, **64**, 549.
29. M. K. Jang, A. Hartwig and B. K. Kim, *J. Mater. Chem.*, 2009, **19**, 1166.
30. C. Y. Bae, J. H. Park, E. Y. Kim, Y. S. Kang and B. K. Kim, *J. Mater. Chem.*, 2011, **21**, 11288.
31. Y. Zhang, Q. Wang, C. Wang and T. Wang, *J. Mater. Chem.*, 2011, **21**, 9073.
32. K. Y. Mya, H. B. Gose, T. Pretsch, M. Bothe and C. He, *J. Mater. Chem.*, 2011, **21**, 4827.
33. M. Bothe, K. Y. Mya, E. M. J. Lin, C. C. Yeo, X. Lu, C. He and T. Pretsch, *Soft Matter*, 2012, **8**, 965.

34. S. A. Dai, T. Y. Juang, C. P. Chen, H. Y. Chang, W. J. Kuo, W. C. Su and R. J. Jeng, *J. Appl. Polym. Sci.*, 2007, **103**, 3591.

35. J. K. Liu, S. M. Shau, T. Y. Juang, C. C. Chang, S. A. Dai, W. C. Su, C. H. Lin and R. J. Jeng, *J. Appl. Polym. Sci.*, 2011, **120**, 2411.

36. C. C. Tsai, T. Y. Juang, S. A. Dai, T. M. Wu, W. C. Su, Y. L. Liu and R. J. Jeng, *J. Mater. Chem.*, 2006, **16**, 2056.

37. Y. C. Chen, T. Y. Juang, S. A. Dai, T. M. Wu, J. J. Lin and R. J. Jeng, *Macromol. Rapid Commun.*, 2008, **29**, 535.

38. B. C. Chun, M. H. Chong and Y. C. Chung, *J. Mater. Sci.*, 2007, **42**, 6524.

39. K. Paderni, S. Pandini, S. Passera, F. Pilati, M. Toselli and M. Messori, *J. Mater. Sci.*, 2012, **47**, 4354.

40. L. Xue, S. Dai and Z. Li, *Macromolecules*, 2009, **42**, 964.

41. C. C. Tsai, C. C. Chang, C. S. Yu, S. A. Dai, T. M. Wu, W. C. Su, C. N. Chen, F. M. C. Chen and R. J. Jeng, *J. Mater. Chem.*, 2009, **19**, 8484.

42. Y. A. Su, W. F. Chen, T. Y. Juang, W. H. Ting, T. Y. Liu, C. F. Hsieh, S. A. Dai and R. J. Jeng, *Polymer*, 2014, **55**, 1481.

43. Y. C. Chen, T. Y. Juang, T. M. Wu, S. A. Dai, W. J. Kuo, Y. L. Liu, F. M. C. Chen and R. J. Jeng, *ACS Appl. Mater. Interfaces*, 2009, **1**, 2371.

44. C. J. Wubg, K. S. Lee, P. N. Prasad, J. C. Kim, J. I. Jin and H. K. Shim, *Polymer*, 1992, **33**, 4145.

45. P. A. Davis, L. Nicolais, L. Ambrosio and S. J. Huang, *J. Bioact. Compat. Polym.*, 1988, **3**, 205.

46. R. Hill and E. E. Walker, *J. Polym. Sci.*, 1948, **3**, 609.

47. C. L. Huang, L. Jiao, J. J. Zhang, J. B. Zeng, K. K. Yang and Y. Z. Wang, *Polym. Chem.*, 2012, **3**, 800.

48. C. Sivakumar and A. Sultan Nasar, *J. Appl. Polym. Sci.*, 2011, **120**, 725.

49. P. Ping, W. Wang, X. Chen and X. Jing, *J. Polym. Sci. Part B: Polym. Phys.*, 2007, **45**, 557.

Figure captions

Table 1. Formulations, compositions, and average molecular weights of LPUs, SPUs, and CPUs.

Table 2. Thermal properties of LPUs, SPUs, and CPUs.

Table 3. Mechanical properties of LPUs, SPUs, and CPUs.

Table 4. Shape memory properties of LPUs, SPUs, and CPUs.

Scheme 1. Synthesis route of 4-isocyanate-4′-(3,3-dimethyl-2,4-dioxo-azetidine)diphenyl methane based diol (IDD-diol).

Scheme 2. Synthesis routes of MDI and PCL based LPUs and SPUs.

Scheme 3. Synthesis routes of CPUs crosslinked with alkoxysilanes and 1,6-diaminohexane.

Fig. 1. Schematic representations of CPUs with different kinds of chemical crosslinking networks ((a) PU laterally crosslinked with flexible long chains, (b) PU laterally crosslinked with short rigid linkages, (c) PU crosslinked with organic multifunctional units, (d) PU/silica composite, (e) PU laterally crosslinked by sol-gel reactions without the addition of fumed silica particles, (f) PU laterally crosslinked by sol-gel reactions with the addition of fumed silica particles, (g) PU crosslinked by sol-gel reactions with the addition of fumed silica particles, and (h) PU crosslinked with POSS based multifunctional units).

Fig. 2. FTIR spectra of LPU55, SPU55, CPU55-A10, and CPU55-S60.

Fig. 3. DSC thermograms of (a) LPUs (LPU45, LPU50, and LPU55) and SPUs (SPU45, SPU50, and SPU55), and (b) CPUs (CPU55-A05, CPU55-A10, CPU55-S20, CPU55-S40, and CPU55-S60) measured at a heating and cooling rate of 10 °C min^{-1}.

Fig. 4. X-ray diffraction patterns of (a) LPUs (LPU45, LPU50, and LPU55) and SPUs (SPU45, SPU50, and SPU55), and (b) CPUs (CPU55-A05, CPU55-A10, CPU55-S20, CPU55-S40, and CPU55-S60).

Fig. 5. Stress-strain curves of (a) LPUs (LPU45, LPU50, and LPU55) and SPUs (SPU45, SPU50, and SPU55), and (b) CPUs (CPU55-A05, CPU55-A10, CPU55-S20, CPU55-S40, and CPU55-S60) measured by a tensile tester with a cross-head speed of 100 mm/min at room temperature.

Fig. 6. Temperature dependence of the (a) storage modulus, and (b) tanδ for PUs measured at 1 Hz by a dynamic mechanical analyzer.

Fig. 7. Cyclic loading and unloading test of shape memory PUs (the loading strain ε_m = 100%; the deformation temperature T_{def} = 70 ^oC; the fixing temperature T_{fix} = 10 ^oC).

Fig. 8. Photographs for the stepwise recovery progress from temporary shape (spiral) to permanent shape (strip) at 70 ^oC for the LPU55, SPU55, CPU55-A10, CPU55-S20, CPU55-40, and CPU55-S60.

Fig. 9. Shape recovery times of the deformed PUs at 70 ^oC.

Table 1. Formulations, composition, and average molecular weights of LPUs, SPUs, and CPUs.

Samples	DEG[a] (mole)	IDD-diol[b] (mole)	PCL-3000 (mole)	MDI (mole)	Crosslinker[c] (mole)	APTS[d] (mole)	Mw(10^4)	PDI
LPU45	1	0	0.16	1.16	—	—	6.84	3.1
LPU50	1	0	0.13	1.13	—	—	7.03	3.4
LPU55	1	0	0.10	1.10	—	—	8.13	3.2
SPU45	0	1	0.31	1.31	—	—	13.68	3.9
SPU50	0	1	0.24	1.24	—	—	10.27	4.4
SPU55	0	1	0.20	1.20	—	—	14.20	4.1
CPU45-A05	0	1	0.31	1.31	0.05	—	—	—
CPU45-A10	0	1	0.31	1.31	0.10	—	—	—
CPU50-A05	0	1	0.24	1.24	0.05	—	—	—
CPU50-A10	0	1	0.24	1.24	0.10	—	—	—
CPU55-A05	0	1	0.20	1.20	0.05	—	—	—
CPU55-A10	0	1	0.20	1.20	0.10	—	—	—
CPU55-S20	0	1	0.20	1.20	—	0.20	—	—
CPU55-S40	0	1	0.20	1.20	—	0.40	—	—
CPU55-S60	0	1	0.20	1.20	—	0.60	—	—

[a] DEG: chain extender for LPUs.
[b] IDD-diol: chain extender for SPUs.
[c] Crosslinking agent: 1, 6-diaminohexane.
[d] Crosslinking agent: APTS.

Table 2. Thermal properties of LPUs, SPUs, and CPUs.

PUs[a]	T_d[b] (°C)	T_g[c] (°C)	T_{cS}[d] (°C)	X_{cS}[e] (%)	T_{mS}[f] (°C)	X_{mS}[g]	T_{mH}[h] (°C)
LPU45	257	−48.3	−1.1	8	37.4	7	141.6
LPU50	270	−48.3	−1.1	8	37.9	7	142.9
LPU55	262	−46.9	N/A	N/A	37.3	1	142.1
SPU45	242	−44.6	13.4	19	43.1	24	N/A
SPU50	244	−45.4	10.5	23	40.1	26	N/A
SPU55	247	−42.0	9.7	22	42.1	24	N/A
CPU45-A05	248	−46.6	10.2	22	41.9	27	N/A
CPU45-A10	263	−47.2	6.5	21	42.9	27	N/A
CPU50-A05	253	−47.4	6.5	22	43.2	28	N/A
CPU50-A10	254	−44.6	10.9	22	42.2	27	N/A
CPU55-A05	249	−41.3	12.2	21	42.5	23	N/A
CPU55-A10	252	−39.2	16.8	20	41.3	21	N/A
CPU55-S20	247	−45.4	16.9	11	40.1	21	N/A
CPU55-S40	250	−38.6	11.6	13	41.9	15	N/A
CPU55-S60	252	−45.8	9.2	13	41.6	13	N/A

[a]: 5-10 mg of film-like sample with ~40 μm.

[b] T_d: degradation temperature (5% weight loss in N_2).

[c] T_g: glass-transition temperature.

[d] T_{cS}: recrystallization temperature of soft segments based domains.

[e] X_{cS}: recrystallization degree of soft segments based domains; calculated according to $(\Delta H_c/H_{c,100\%}) \times 100\%$, where $H_{c,100\%}$ is the recrystallization enthalpy of PCL (−80.2 mJ/mg).

[f] T_{mS}: melting temperature of soft segments based domains.

[g] $X_{mS:}$ crystallization degree of soft segment based domains; calculated according to $(\Delta H_{mS}/H_{mS,100\%}) \times 100\%$, where $H_{mS,100\%}$ is the melting enthalpy of PCL (82.9 mJ/mg).

[h] T_{mH}: melting temperature of hard segment based domains.

Table 3. Mechanical properties of LPUs, SPUs, and CPUs.

PUs	σ_b[a] (MPa)	σ_b[b] (MPa)	ε_b[c] (%)	E_e[d] (MPA)	E_s[e] (MPA)	E'_g[f] (MPa)	E'_r[g] (MPa)	$Tan_{max}\delta$[h]
LPU45	7.3±0.6	58.0±3.7	510±24.0	1.5±03	0.07±0.02	150.5±20.1	47.1±1.4	0.20±0.03
LPU50	19.2±1.1	70.1±4.1	500±22.7	5.8±0.4	0.19±0.03	289.6±12.4	71.3±2.1	0.15±0.01
LPU55	21.1±1.1	107.0±8.7	423±37.1	5.4±0.3	0.21±0.04	442.5±11.9	110.2±5.0	0.14±0.02
SPU45	1.4±0.2	19.6±1.6	481±34.5	0.3±0.1	0.02±0.01	870.6±55.2	1.7±0.2	0.90±0.08
SPU50	4.5±0.3	30.1±2.2	400±23.8	0.8±0.2	0.05±0.01	1041.5±93.1	4.3±0.4	0.89±0.11
SPU55	5.5±0.8	45.4±2.9	363±15.6	1.1±0.2	0.06±0.01	650.2±20.8	2.6±0.1	0.89±0.13
CPU45-A05	1.5±0.2	24.1±2.1	462±25.2	0.8±0.2	0.05±0.02	815.3±33.8	1.7±0.1	0.85±0.16
CPU45-A10	1.7±0.1	27.3±2.4	454±18.4	2.2±0.3	0.09±0.02	925.2±32.0	3.6±0.2	0.77±0.13
CPU50-A05	5.6±0.4	38.3±3.8	375±22.6	1.2±0.2	0.07±0.01	916.5±28.5	4.9±0.1	0.80±0.03
CPU50-A10	7.4±0.8	39.8±4.0	361±24.3	2.8±0.4	0.10±0.03	1093.4±65.6	3.8±0.1	0.80±0.15
CPU55-A05	9.1±0.7	41.5±2.7	335±14.3	2.2±0.2	0.07±0.02	1610.4±89.4	6.4±0.3	0.85±0.17
CPU55-A10	12.0±1.2	51.0±4.2	306±24.9	3.2±0.4	0.11±0.03	2334.5±125.1	8.1±0.6	0.80±0.01
CPU55-S20	15.5±1.3	45.8±3.1	241±12.0	2.8±0.3	0.14±0.03	1276.8±82.3	14.1±1.4	0.78±0.06
CPU55-S40	26.5±1.7	34.2±2.6	127±7.3	6.0±0.4	0.26±0.04	1664.7±86.7	27.2±1.0	0.63±0.10
CPU55-S60	38.2±2.1	41.6±2.9	106±8.9	8.0±0.5	0.38±0.04	1765.5±103.5	55.9±2.1	0.56±0.02

[a] Tensile stress at 100% elongation
[b] Tensile stress at break
[c] Elongation at break
[d] Elastic modulus
[e] Secant modulus: defined as the slope of the line connecting the origin and a given point (at 100% elongation) on the stress-strain curve.
[f] E'_g: at 10 ^oC measured from DMA curves.
[g] E'_r: at 70 ^oC measured from DMA curves.
[h] $Tan_{max}\delta$ at 70 ^oC measured from DMA curves.

Table 4. Shape memory properties of LPUs, SPUs, and CPUs.

PUs	Shape recovery (%)			Shape retention (%)		
	1st	2nd	3rd	1st	2nd	3rd
LPU45	79.2±2.1	69.5±1.5	54.0±2.2	80.6±1.9	66.1±2.0	61.2±1.8
LPU50	84.3±4.4	68.9±3.1	67.8±2.5	81.3±1.4	71.7±3.3	70.6±2.8
LPU55	88.4±2.1	77.8±3.5	78.7±2.7	76.1±2.2	71.7±2.1	67.2±1.4
SPU45	79.4±2.2	77.4±3.2	73.4±3.3	76.1±3.4	72.8±3.0	66.1±1.7
SPU50	90.5±3.0	72.0±2.4	72.5±2.1	95.1±3.4	92.2±3.7	91.1±2.8
SPU55	91.4±2.7	87.3±2.9	84.4±1.4	90.0±2.5	87.6±2.6	85.6±1.4
CPU45-A05	94.0±2.9	83.4±3.4	78.4±3.2	71.7±1.6	66.2±2.4	61.1±3.1
CPU45-A10	97.5±2.6	94.8±3.7	90.0±2.2	81.7±3.1	76.1±2.6	75.6±2.1
CPU50-A05	97.9±3.2	97.3±2.8	92.5±3.0	90.3±1.8	89.3±1.9	87.2±2.5
CPU50-A10	98.9±2.7	97.8±3.1	93.5±3.1	86.2±0.9	85.6±2.3	85.0±2.6
CPU55-A05	95.5±4.2	92.5±1.7	92.5±3.9	90.5±2.2	86.1±3.8	85.0±2.2
CPU55-A10	99.5±3.8	98.4±1.2	97.5±3.7	87.6±3.1	86.7±4.0	85.0±1.9
CPU55-S20	99.5±2.5	97.5±3.8	97.5±2.9	95.0±2.7	92.8±2.9	91.5±1.6
CPU55-S40	99.8±3.4	99.5±2.6	99.4±2.0	90.0±2.0	87.8±2.1	87.5±2.7
CPU55-S60	99.8±4.1	99.8±2.3	—[a]	85.0±2.8	83.6±2.2	—[a]

[a] Sample was fractured.

31x12mm (600 x 600 DPI)

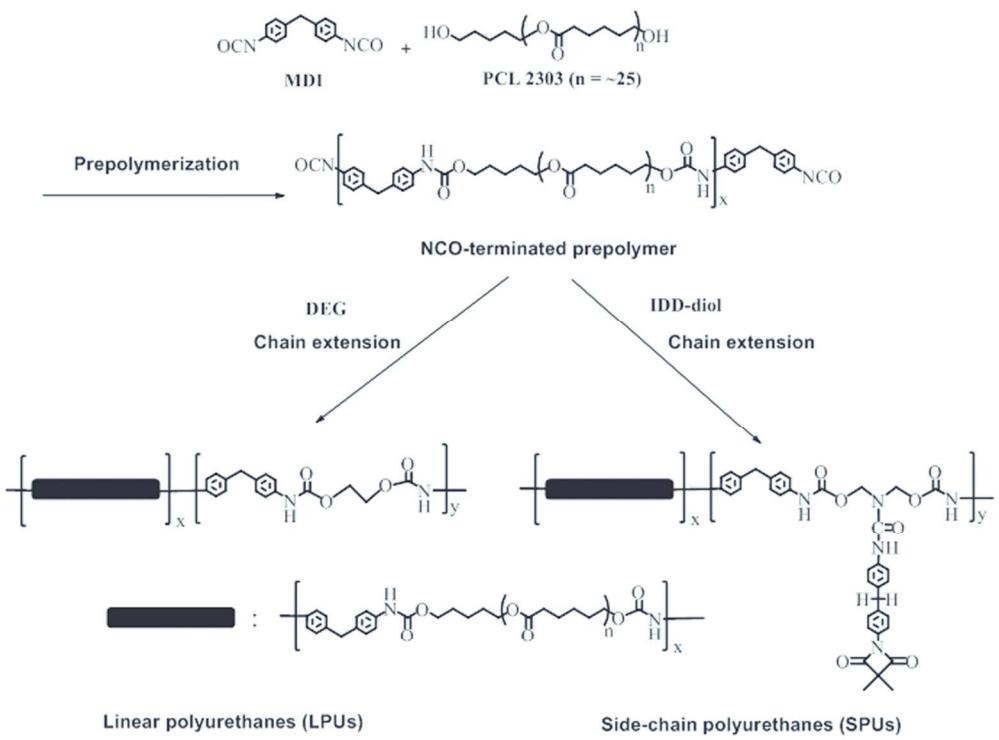

Synthesis routes of MDI and PCL based LPUs and SPUs.
61x45mm (600 x 600 DPI)

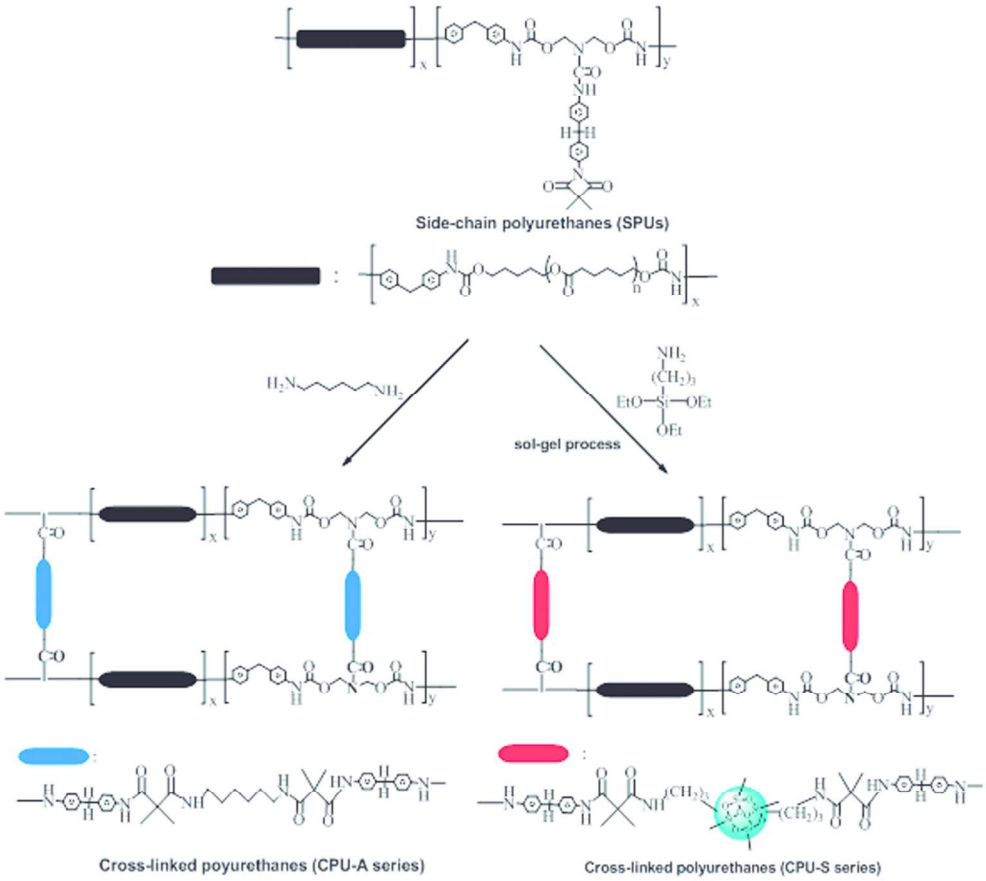

Synthesis routes of CPUs crosslinked with alkoxysilanes and 1,6-diaminohexane.
73x65mm (600 x 600 DPI)

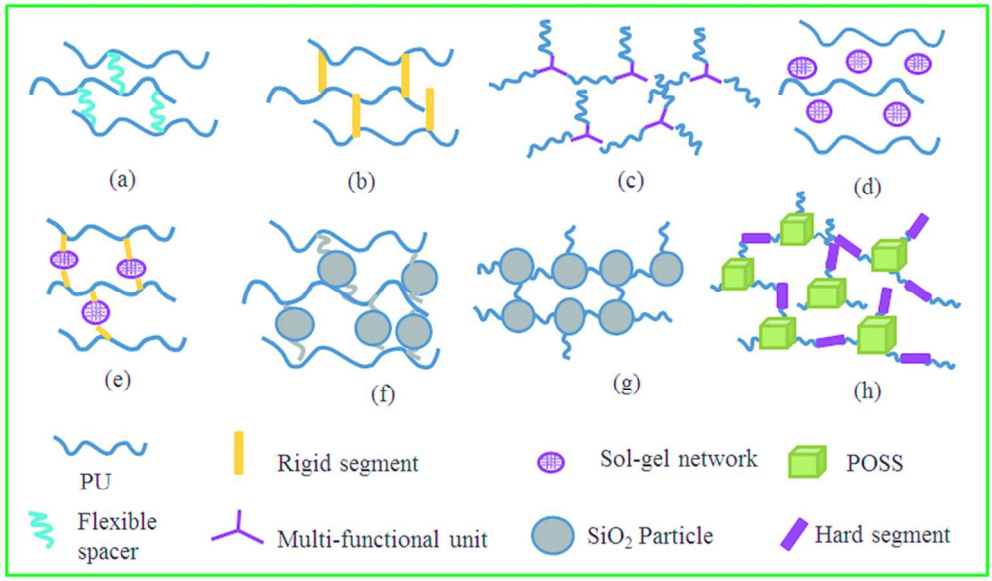

Schematic representations of CPUs with different kinds of chemical crosslinking networks ((a) PU laterally crosslinked with flexible long chains, (b) PU laterally crosslinked with short rigid linkages, (c) PU crosslinked with organic multifunctional units, (d) PU/silica composite, (e) PU laterally crosslinked by sol-gel reactions without the addition of fumed silica particles, (f) PU laterally crosslinked by sol-gel reactions with the addition of fumed silica particles, (g) PU crosslinked by sol-gel reactions with the addition of fumed silica particles, and (h) PU crosslinked with POSS based multifunctional units).
48x28mm (600 x 600 DPI)

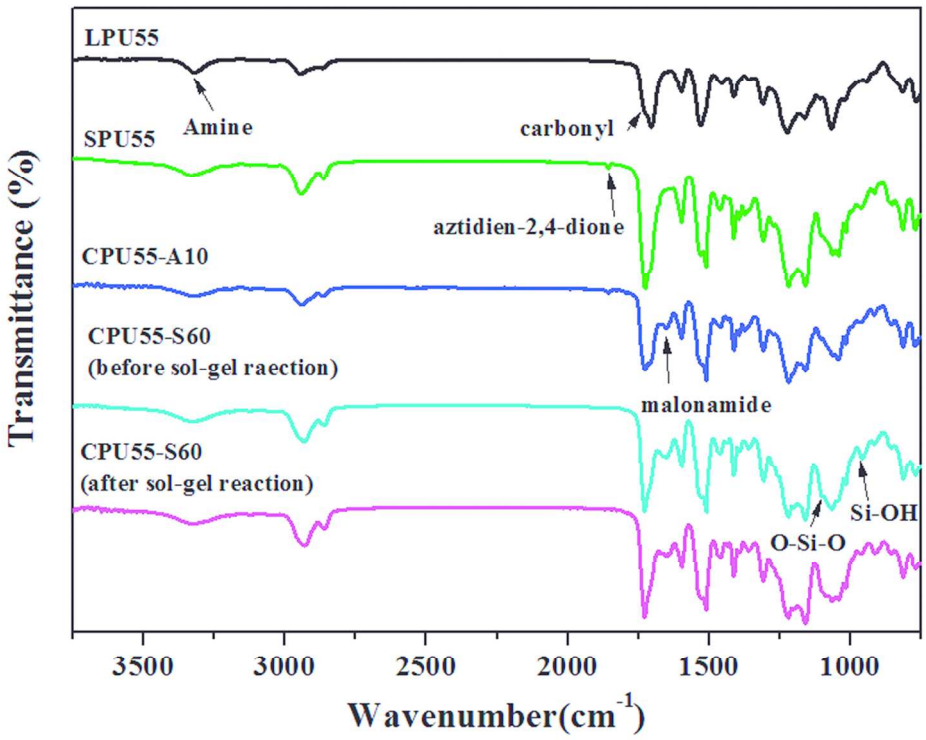

FTIR spectra of LPU55, SPU55, CPU55-A10, and CPU55-S60.
63x48mm (600 x 600 DPI)

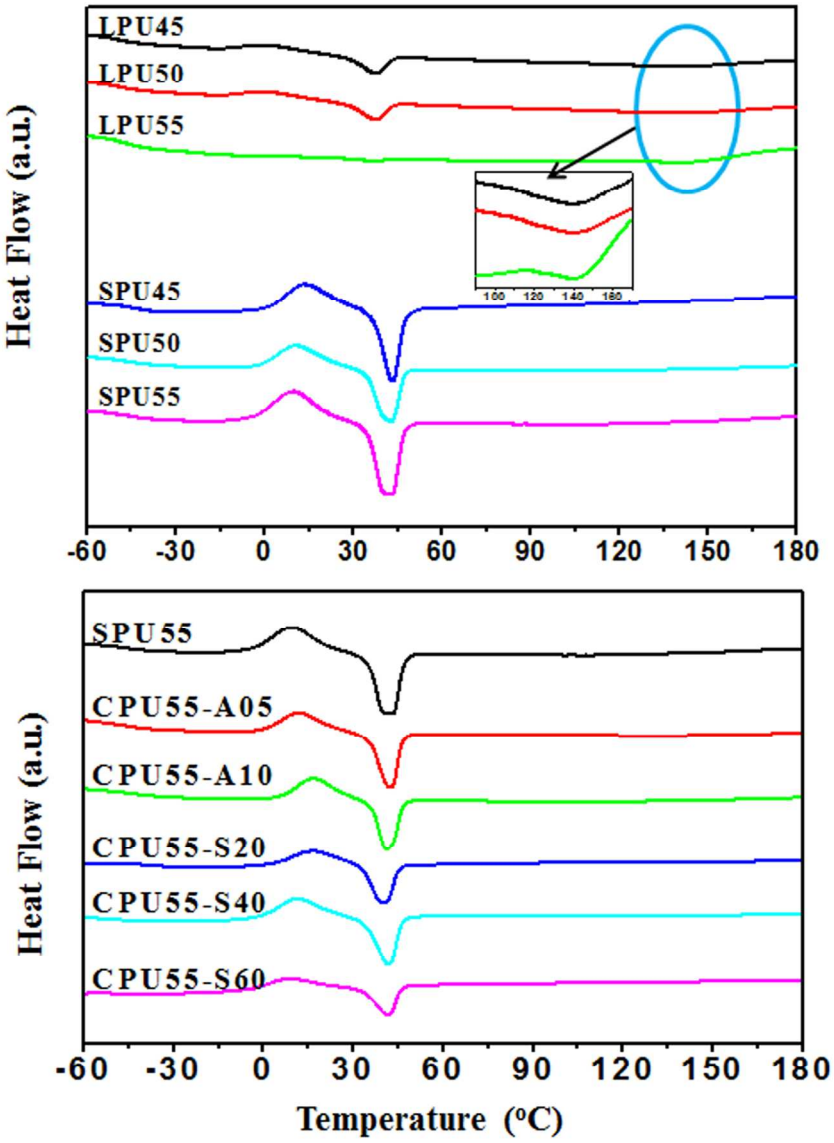

DSC thermograms of (a) LPUs (LPU45, LPU50, and LPU55) and SPUs (SPU45, SPU50, and SPU55), and (b) CPUs (CPU55-A05, CPU55-A10, CPU55-S20, CPU55-S40, and CPU55-S60) measured at a heating and cooling rate of 10 ?C min?1.
108x142mm (600 x 600 DPI)

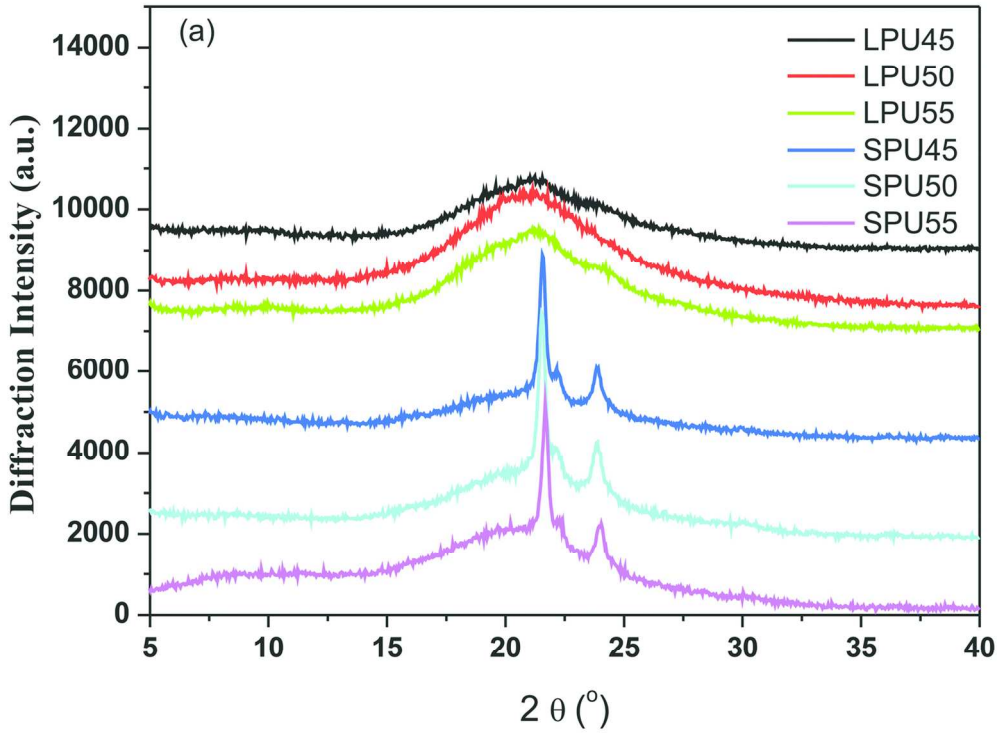

X-ray diffraction patterns of (a) LPUs (LPU45, LPU50, and LPU55) and SPUs (SPU45, SPU50, and SPU55), and (b) CPUs (CPU55-A05, CPU55-A10, CPU55-S20, CPU55-S40, and CPU55-S60).
65x51mm (600 x 600 DPI)

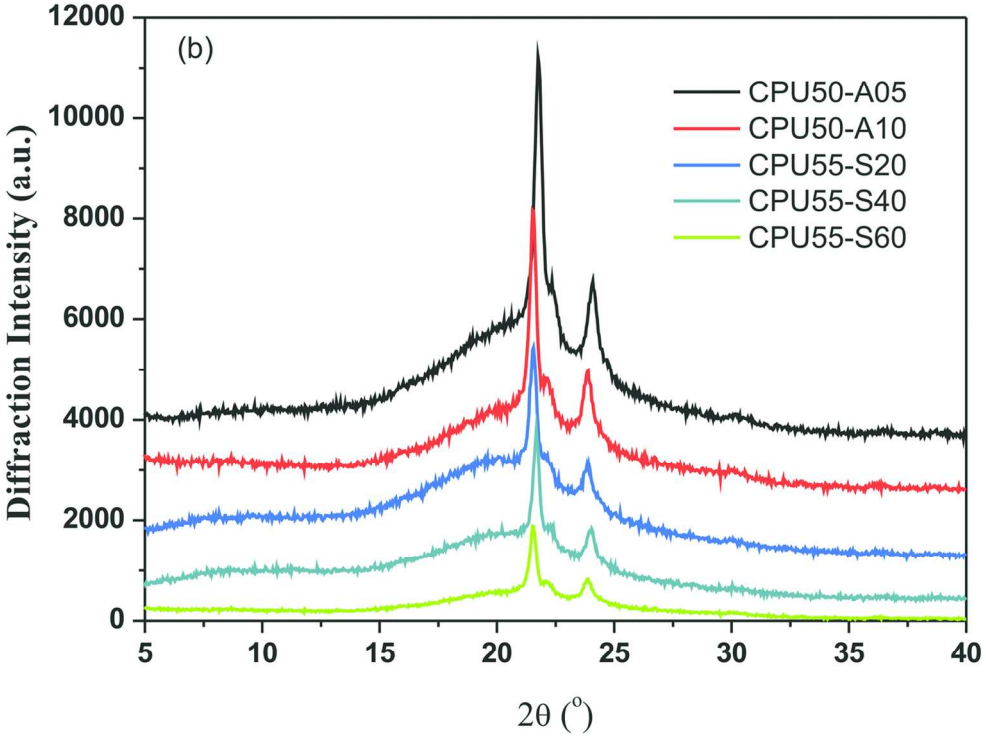

X-ray diffraction patterns of (a) LPUs (LPU45, LPU50, and LPU55) and SPUs (SPU45, SPU50, and SPU55), and (b) CPUs (CPU55-A05, CPU55-A10, CPU55-S20, CPU55-S40, and CPU55-S60).
62x46mm (600 x 600 DPI)

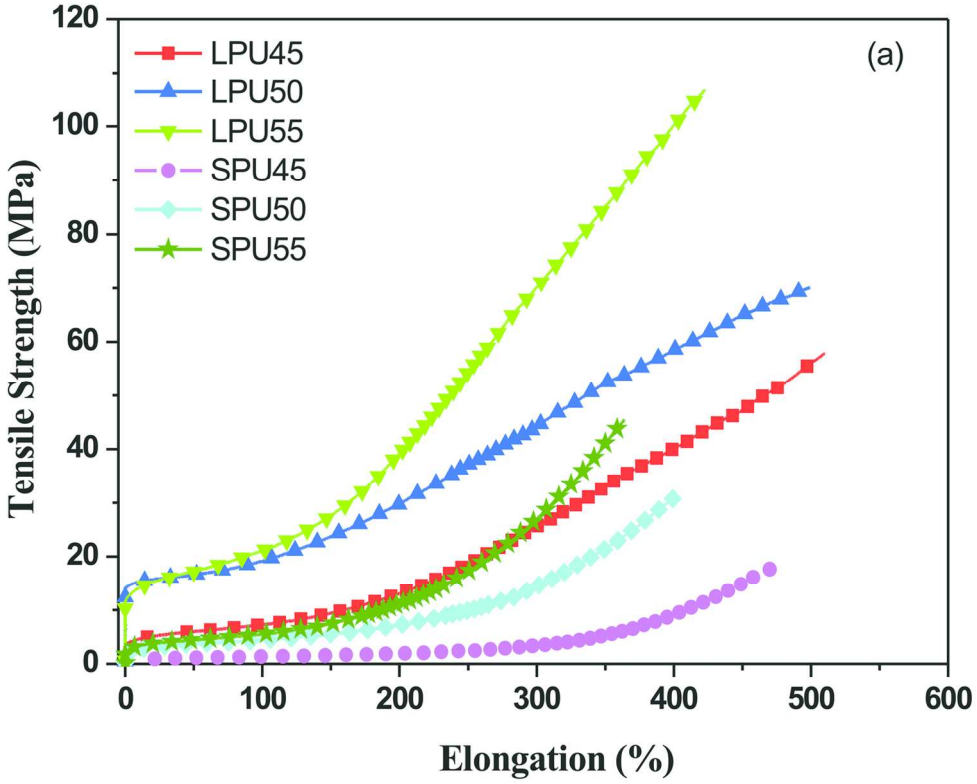

Stress-strain curves of (a) LPUs (LPU45, LPU50, and LPU55) and SPUs (SPU45, SPU50, and SPU55), and (b) CPUs (CPU55-A05, CPU55-A10, CPU55-S20, CPU55-S40, and CPU55-S60) measured by a tensile tester with a cross-head speed of 100 mm/min at room temperature.
66x53mm (600 x 600 DPI)

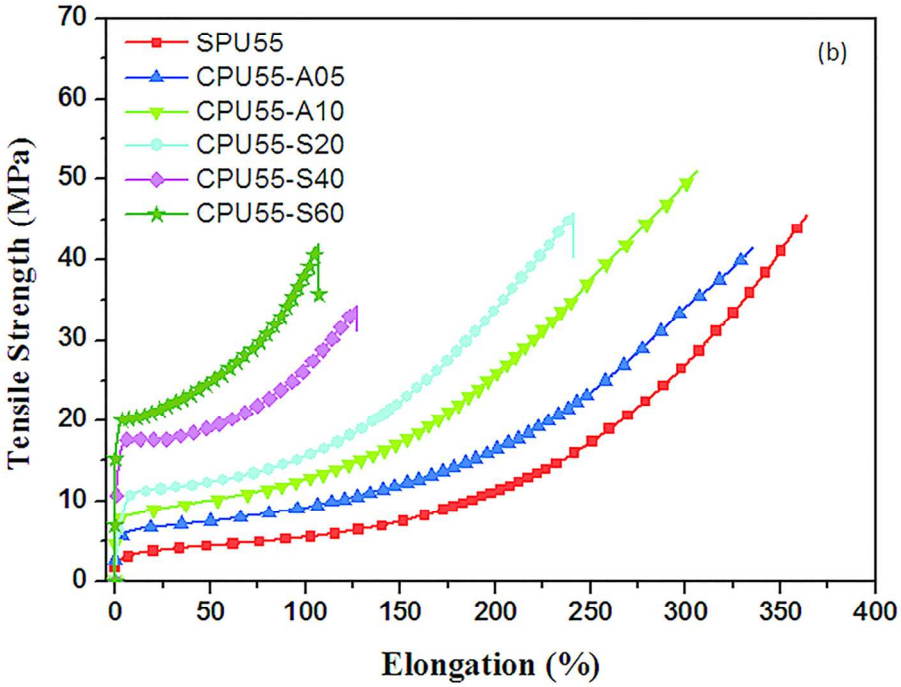

Stress-strain curves of (a) LPUs (LPU45, LPU50, and LPU55) and SPUs (SPU45, SPU50, and SPU55), and (b) CPUs (CPU55-A05, CPU55-A10, CPU55-S20, CPU55-S40, and CPU55-S60) measured by a tensile tester with a cross-head speed of 100 mm/min at room temperature.
62x47mm (600 x 600 DPI)

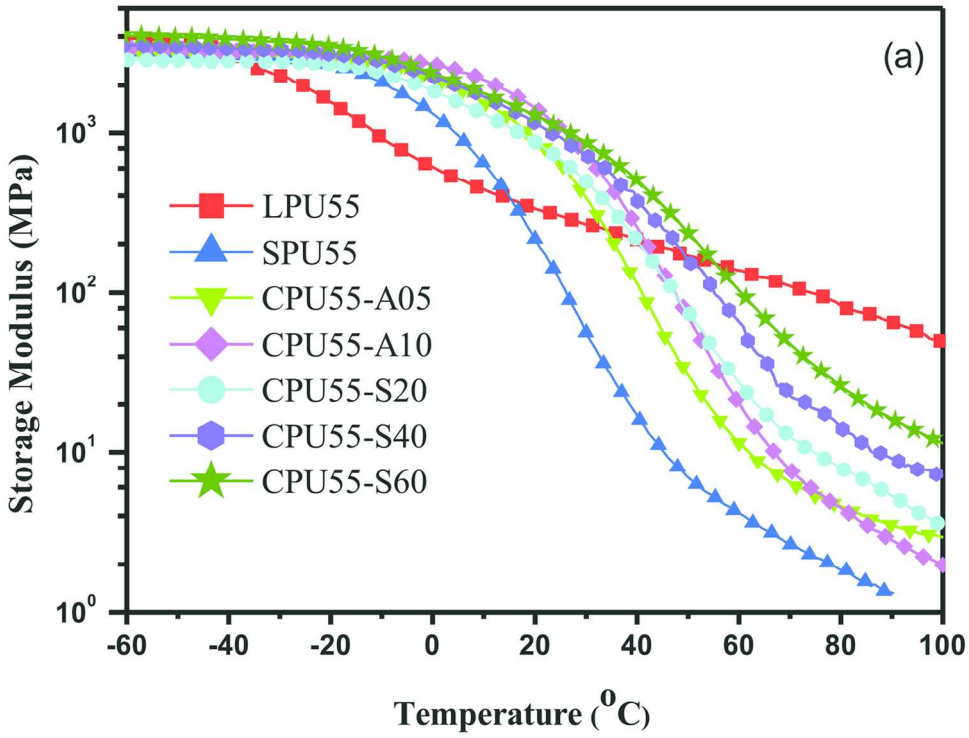

Temperature dependence of the (a) storage modulus, and (b) tanδ for PUs measured at 1 Hz by a dynamic mechanical analyzer.
63x49mm (600 x 600 DPI)

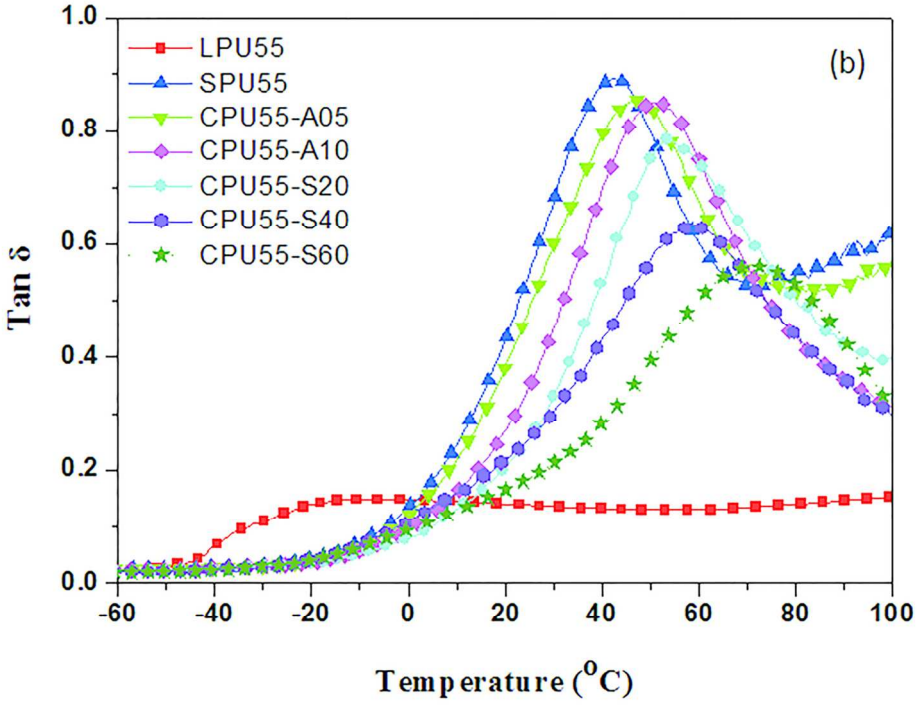

Temperature dependence of the (a) storage modulus, and (b) tanδ for PUs measured at 1 Hz by a dynamic mechanical analyzer.
64x50mm (600 x 600 DPI)

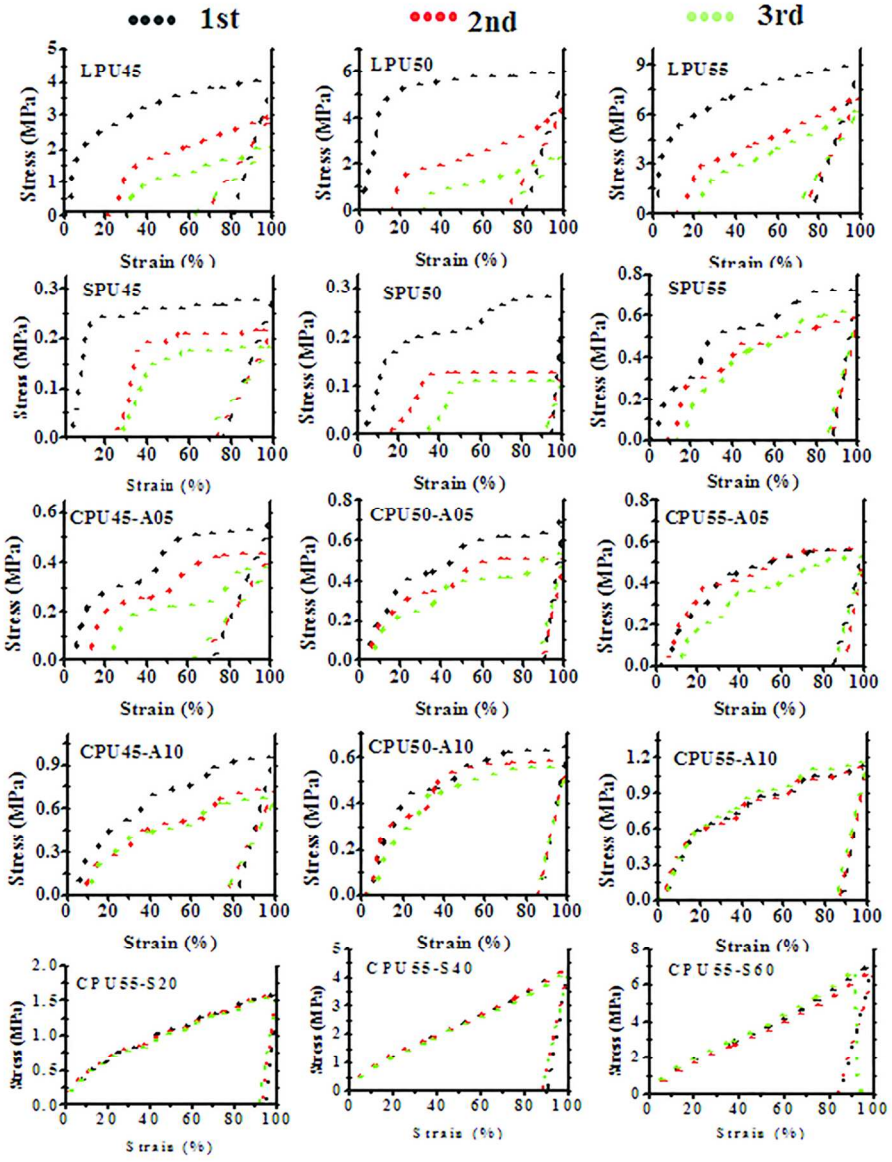

Cyclic loading and unloading test of shape memory PUs (the loading strain εm = 100%; the deformation temperature Tdef = 70 oC; the fixing temperature Tfix = 10 oC).
67x87mm (600 x 600 DPI)

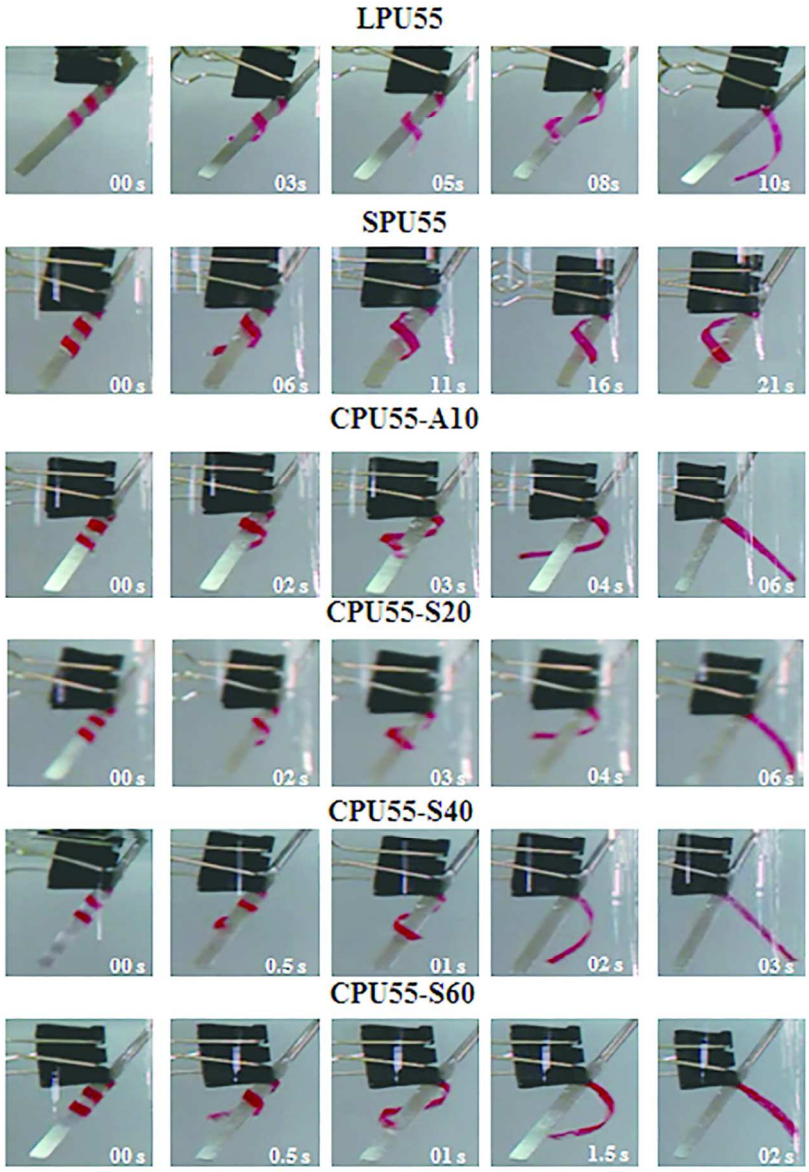

Photographs for the stepwise recovery progress from temporary shape (spiral) to permanent shape (strip) at 70 oC for the LPU55, SPU55, CPU55-A10, CPU55-S20, CPU55-40, and CPU55-S60.
73x104mm (600 x 600 DPI)

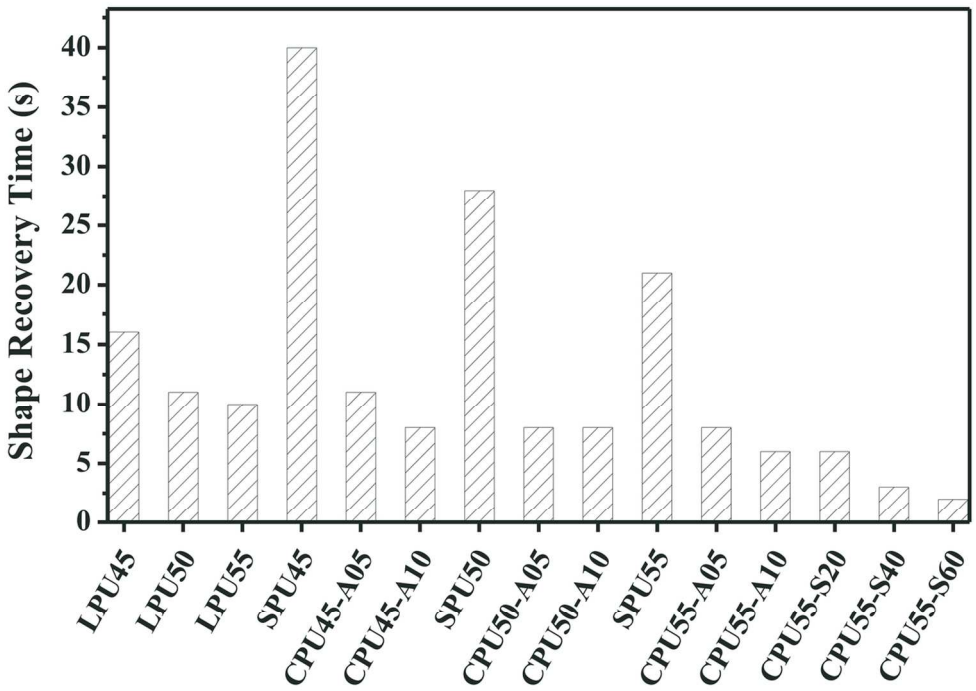

Shape recovery times of the deformed PUs at 70 oC.
59x42mm (600 x 600 DPI)